JOURNAL OF MATERIALS SCIENCE 21 (1986) 395–404

# Formation of compounds by high-flux nitrogen ion implantation in titanium

BERND RAUSCHENBACH
*Academy of Science of GDR, Central Institute of Nuclear Research, Rossendorf, Box 19, 8051 Dresden, German Democratic Republic*

Polycrystalline titanium was implanted with nitrogen ions at energies from 30 to 60 keV and with doses from $1 \times 10^{16}$ to $1.5 \times 10^{18}$ $N^+$-ions $cm^{-2}$ at room temperature. The implanted titanium layers were investigated by high-voltage electron microscopy and transmission high-energy electron diffraction. The formation of titanium nitride, titanium carbonitride and titanium carbide phases were considered in relation to their dependence on nitrogen ion implantation dose. In the dose range from $1 \times 10^{16}$ up to $1.5 \times 10^{18}$ $N^+$-ions $cm^{-2}$ the cubic phase $\delta$-$TiN_x$ was formed. In the dose range between 1 to $2.5 \times 10^{17}$ and $1.5 \times 10^{18}$ $N^+$-ions $cm^{-2}$ the tetragonal phase $\varepsilon$-$Ti_2N$ was found in addition to the $\delta$-$TiN_x$ phase. The lattice structure of these titanium nitride phases is a function of the nitrogen ion implantation dose. Additionally, the presence of titanium carbonitride $TiC_yN_x$ and titanium carbide $TiC_y$ phases can be proved. The analysed titanium nitride, titanium carbonitride and titanium carbide phases are represented in a state diagram as a function of implantation dose.

## 1. Introduction

In recent years the high-flux implantation of metalloid ions (nitrogen, carbon, boron) has been applied to various metallic targets in order to improve their mechanical properties such as wear, fatigue, hardness etc. (e.g. [1]). Consequently, basic investigations of ion implantation metallurgy are essential so as to use this technique effectively.

Thin-film layers of titanium nitride are of great interest in a wide range of technological applications. For example, titanium nitride has interesting mechanical (extreme hardness), thermal (high melting point), chemical (high corrosion resistance) and electrical properties. Therefore titanium nitride has been used to make hard wear-reducing coatings on tools, high-temperature structural materials, miniature resistive and capacitative electronic components, basic materials for solar energy technology, etc. In general, titanium nitride is obtained either by chemical vapour deposition [2] or by reactive physical vapour deposition [3].

The object of this paper is to analyse the titanium nitride compounds obtained after high-flux nitrogen ion implantation into titanium. So far only a few papers are known which have analysed the phases after nitrogen ion implantation [4–8]. Bykov *et al.* [4] and Belii *et al.* [5] found TiN after nitrogen ion implantation of $1 \times 10^{17}$ and $4 \times 10^{17}$ $N^+$-ions $cm^{-2}$ into titanium by the use of electron diffraction. With the help of X-ray diffraction and Rutherford backscattering Duckworth and Wilson [7] found titanium nitride after 600 keV nitrogen ion implantation, and Chen and Yang [6] could detect the (1 1 1) reflection of the cubic TiN phase after implantation of $3 \times 10^{15}$ $N^+$-ions $cm^{-2}$ or $9 \times 10^{16}$ $N^+$-ions $cm^{-2}$ into titanium.

## 2. Experimental conditions

Polycrystalline layers of titanium were deposited on freshly cleaved NaCl or KCl, and on silicon in a high vacuum of $10^{-3}$ Pa. The thickness of the layers was varied between 100 nm and 1 $\mu$m. The titanium films were implanted at room temperature with nitrogen ions with energies from 30 to 60 keV in the dose range of $1 \times 10^{16}$ to $1.5 \times 10^{18}$ $N^+$-ions $cm^{-2}$. A lateral homogeneous distribution of nitrogen was obtained by a wobbled nitrogen ion beam. The typical dose rate was $< 5\,\mu A\,cm^{-2}$. The choice of a low dose rate is important for a low heating of the specimens during implantation. The temperatures during implantation were kept below 50° C. Auger electron spectrometry (AES) measurements were performed to analyse the implantation profiles and impurity contents (carbon, oxygen) of unimplanted and implanted titanium targets [8, 9]. Measurements with the aid of AES showed that the accuracy of ion dose was better than 92%.

The crystallographic structure and morphology of the titanium layers before and after implantation were investigated by high-voltage electron microscopy (HVEM) and transmission high-energy electron diffraction (THEED). Studies were made by the use of a 1 MeV electron microscope (JEM – 1000) and the selected-area diffraction (SAD) technique. A problem at high voltages (> 300 to 500 keV) is knock-on displacement damage. Our experiments show that this damage is negligible under our operating conditions (small electron flux, low temperature).

Identification of phases after implantation took place on the basis of electron scattering diffraction diagrams. The electron scattering curves were obtained by calibrated selected-area diffraction patterns. Calibration of SAD patterns is generally straightforward, but can be facilitated by using an internal standard (an

0022–2461/86 $03.00 + .12 

unimplanted region) since the camera constant in the electron microscope is sensitive to change in specimen position.

Diffraction patterns were taken with high-energy electrons. The exposure time was varied stepwise. Exposed plates were developed in order to obtain a wide proportional range of the electron diffraction intensity and the plate darkness. Microphotometer traces of the diffraction patterns were taken with a microphotometer of an automatic balance type. Peak-height intensity was determined in the proportional range of the electron intensity and plate darkness. The distance of Debye–Scherrer rings from the centre of the pattern was also measured with the microphotometer. Using the Bragg equation, the interplanar spacing can be approximated by

$$d_{hkl}^{\exp} = \frac{2\lambda L}{D}\left(1 + \frac{3D}{32L^2}\right) \quad (1)$$

where $D$ is the ring diameter [10]. In our case the camera constant $\lambda L$ was calibrated by comparison with the unimplanted region of an implanted titanium specimen. The accuracy of $\lambda L$ by this procedure is very good.

Computer programs were used to calculate the interplanar spacings, intensities and synthetic electron diffraction spectra. The theoretical values of the interplanar spacings $d_{hkl}^{\text{theo}}$ may be estimated using the Bragg equation, where the wavelength of electrons is corrected with a relativistic term ($\lambda_e = 0.872 \times 10^{-3}$ nm at 1 MeV).

The experimentally determined electron diffraction intensities were compared with theoretically calculated intensities on the basis of the relative intensities, i.e. the intensities normalized by setting that of the most intense reflection to 100. In general, the electron diffraction intensity at temperature $T$ is given by

$$I_{hkl}^{\text{theo}}(T) = C|\Phi_{hkl}^{r}|^2 d_{hkl}^{\text{theo}} \times p \exp[-B(\sin\theta/\lambda_e)^2] f(A) \quad (2)$$

where $C$ is the scale factor, $\Phi_{hkl}^{r}$ is the relativistic structure factor with $\Phi_{hkl}^{r} = (m/m_0)\Phi_{hkl}$, ($m/m_0 = 2.957$ at 1 MeV), $m_0$ is the electron rest mass, $m$ the moving pass, $p$ is the multiplicity, $B$ is the temperature factor [11], $\theta$ is the Bragg angle and $f(A)$ is the primary extinction coefficient [10, 11]. The multiplicity factors for each reflection $hkl$ are from tables [12, 13]. The calculation of structure factors $\Phi_{hkl}$ is for all reflections allowed by the space group [12]. Atomic form factors are obtainable from tables [13, 14]. The extinction conditions are permanently stored in the computer, as tabulated by Herrmann [15]. The agreement of the calculated interplanar spacing with the observed interplanar spacing of the reflections is determined by

$$\varepsilon_d(\%) = 100\left[\frac{(d_{hkl}^{\text{theo}} - d_{hkl}^{\exp})^2}{(d_{hkl}^{\text{theo}})^2}\right]^{1/2} \quad (3)$$

It is known that implantation of metalloid ions lead to the formation of many different phases [16]. Electron diffraction reflections from these phases are partially overlapping. Therefore it is a great problem to determine the positions and intensities of these pekas. The method of Morrey [17] can be used to calculate the positions and intensities of separate electron diffraction reflections. This technique involves the fitting of equidistantly spaced data to a quartic equation and the determination of different derivations of the electron diffraction spectrum. The electron diffraction spectrum is converted into digital data with an analogue-to-digital converter and divided into segments. These segments are fitted with a quartic equation $y = f(z)$, where $z$ is a position relative to a position spanned by the segment. Conditions for the existence of a peak position are $y'' < 0$, $y''' = 0$ and $y'''' > 0$, and the peak position is calculated from

$$y''(z_0) = 2C_1 + 6C_2 z + 12C_3 z^2 < 0 \quad (4)$$

where coefficients $C_i$ can be determined from a set of linear equations derived from a least-squares analysis of the quartic equation (for details and discussion see [17, 18]. A determination of the width and height of each peak can be obtained after the proper roots for $y'''$ and $y''''$ have been found by analysis of the polynomial.

In Fig. 1 this technique is demonstrated with an example of titanium implanted with $2 \times 10^{17}$ $N^+$-ions $cm^{-2}$. The portion $Y$ of the microphotometer curve (Fig. 1a) is divided in different segments after separation of the scattering background (Fig. 1b). The resultant electron diffraction spectrum shows about twelve peaks with a partially asymmetrical form. By applying the method of Morrey [17] it is possible to compute a synthetic spectrum. It is supposed that the distribution of an electron diffraction reflection can be described by a Gaussian distribution function. Mathematically the synthetic spectrum can be represented by a sum of Gaussian distribution functions (Fig. 1c). According to Will *et al.* [19], the goodness-of-fit of the computed to the observed profile is described with a parameter $\varepsilon_f$, similar to the parameter $\varepsilon_d$ of Equation 3. Only if $\varepsilon_f < 5\%$ may the fitted synthetic spectrum be used.

## 3. Results and discussion

Measurements by the use of Auger electron spectroscopy show that the implantation of nitrogen ions into titanium leads to very high nitrogen concentrations (for measurements and discussion see [8, 9]. For example, the maximal nitrogen concentration is $6.5 \times 10^{22}$ $N^+$-ions $cm^{-3}$ at 30 keV and $5 \times 10^{22}$ $N^+$-ions $cm^{-3}$ at 60 keV. Extremely supersaturated titanium targets were used to analyse titanium compounds. Identification of titanium nitride phases was carried out by diffraction contrast (morphology), SAD (lattice structure) and comparison of the measured intensities with calculated intensitites of the diffraction reflections.

Fig. 2 shows SAD, with the bright field (BF) and dark field (DF) images of titanium implanted with $5 \times 10^{16}$ $N^+$-ions $cm^{-2}$. In order to identify the phases of the implanted layer, the approach was used which is demonstrated in Fig. 1. The lattice parameters used for identification of the THEED patterns are compiled in Table I [20–23]. Beside these phases other titanium modifications and compounds

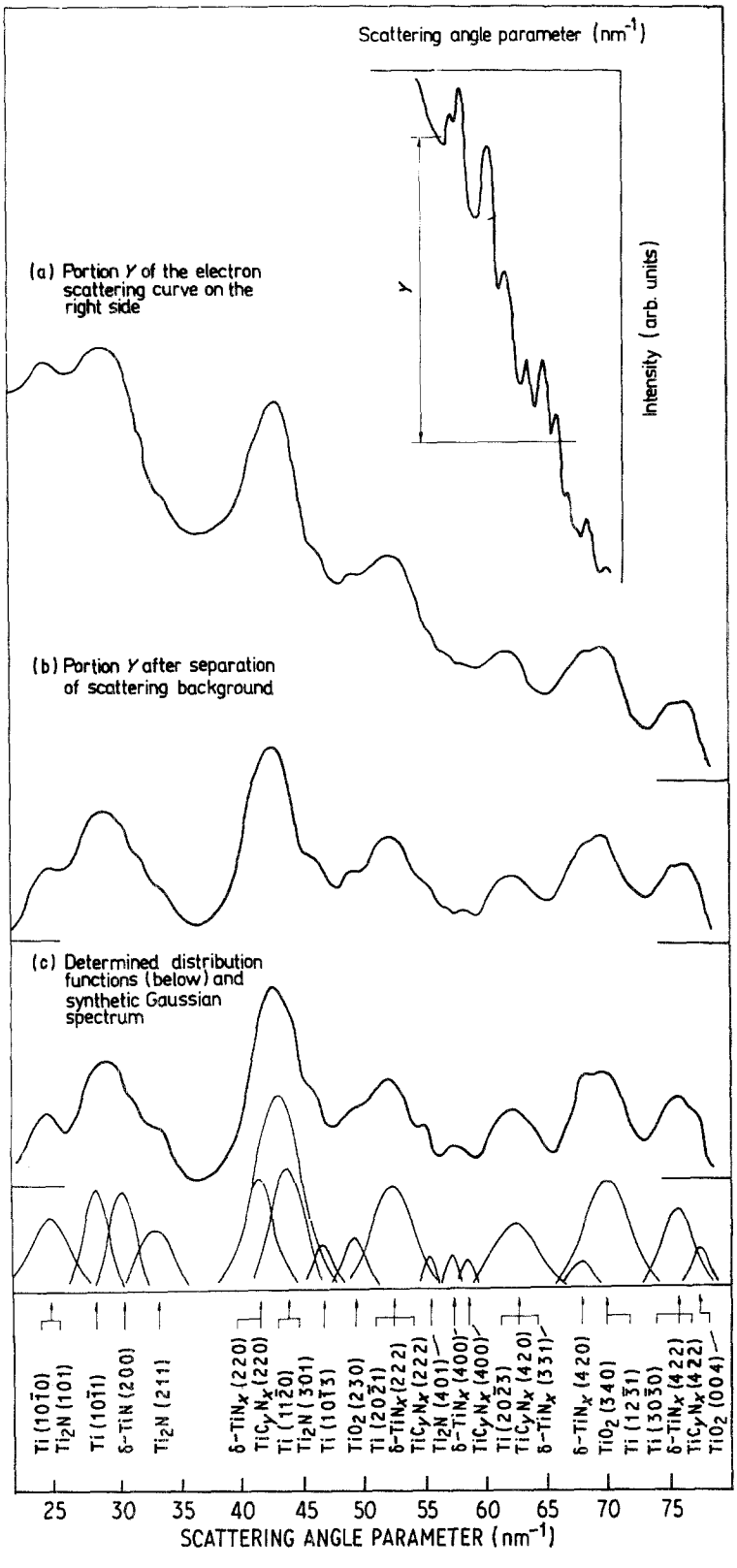


*Figure 1* A typical example used to determine the electron scattering peak positions and synthetic Gaussian spectrum. On the right side the dependence of the electron scattering intensity on the scattering angle parameter is shown for titanium implanted with nitrogen ions to a flux of $2 \times 10^{17}$ N$^+$-ions cm$^{-2}$ at 50 keV and room temperature (25° C). For this example the portion $Y$ of the scattering curve (a) was investigated after subtraction of scattering background (b). Below (c) are the determined distribution functions and the reconstruction of the synthetic Gaussian spectrum. The different titanium compounds found are indicated.

were checked. The allotropic modification of titanium, the high-temperature form $\beta$-Ti (bcc) and high-pressure form $\omega$-Ti (hex), and various titanium oxides, the triclinic structure $Ti_nO_{2n-1}$ ($Ti_7O_{13}$, $Ti_8O_{15}$, $Ti_9O_{17}$), anatase (tetrag.) and brookite (orthorhomb.) could not be identified.

Debye–Scherrer rings from $\alpha$-Ti could be identified in all analysed THEED patterns. The dark precipitates of Fig. 2 (BF) could be identified as the cubic face-centred titanium nitride phase $\delta$-TiN$_x$. This phase can be identified in the dose range from $1 \times 10^{16}$ to $1.5 \times 10^{18}$ N$^+$-ions cm$^{-2}$. The dark-field mode is especially useful in determining the size, distribution and morphology of precipitates. The grain size for the $\delta$-titanium nitride phase is about 40 nm for films near to a stoichiometry of TiN$_{0.5...0.65}$. For layers with a higher nitrogen content (with higher implantation dose) the grains are larger. At an implantation dose of $5 \times 10^{17}$ N$^+$-ions cm$^{-2}$ a grain size of about 150 nm was measured. The grain size is also affected by the implantation dose. Chen and Yang [6] and Duckworth and Wilson [7] also found a cubic titanium nitride phase at similar implantation doses. With other techniques $\delta$-TiN is obtained either by reactive evaporation [24]

TABLE I Crystallographic data for the analysed crystal phases and their lattice parameters

| Phase | Bravais lattice | Short Herrmann–Maugin symbol, Schoenflies symbol | Lattice parameters (nm) | Space group |
|---|---|---|---|---|
| α-Ti | hcp | $P6_3/mmc$, $D^4_{6h}$ | $a = 0.295\,11$<br>$c = 0.468\,43$ | 194 |
| δ-$TiN_x$ | fcc | $Fm\bar{3}m$, $O^5_{6h}$ | $a = 0.421$ to $0.424^{\dagger}$ | 225 |
| ε-$Ti_2N$ | tetrag. | $P4_2/mnm$, $D^{14}_{4h}$ | $a = 0.494\,28$<br>$c = 0.303\,57$ | 136 |
| $TiC_y$ | fcc | $Fm\bar{3}m$, $O^5_{6h}$ | $a = 0.430$ to $0.433^{\dagger}$ | 225 |
| $TiC_yN_x$ | fcc | $Fm\bar{3}m$, $O^5_{6h}$ | $a = 0.423\,8$ to $0.431\,7^{\dagger}$ | 225 |
| $TiO_2$ | tetrag. | $P4_2/mnm$, $D^{14}_{4h}$ | $a = 0.296\,0$<br>$c = 0.459\,0$ | 136 |

$^{\dagger}$Latice parameter is a function of nitrogen and/or carbon content.

or by reactive sputtering [25]. In Table II the interplanar spacings and intensities of the most frequent lattice indices of δ-$TiN_x$ are compiled and compared with theoretical values for two different implantation doses. It can be shown that the experimental interplanar spacings determined from THEED patterns are in good agreement with those obtained by calculations ($\varepsilon_d < 1.4\%$) in dependence on the implantation dose and nitrogen content respectively. Starting from the relationship between the lattice parameter $a$ and nitrogen content in the δ-$TiN_x$ [26] it is possible to derive the nitrogen content with the help of experimentally determined lattice parameters. The lattice parameter for the δ-$TiN_x$ phase, calculated from the interplaner spacings, is shown in Fig. 3 as a function of nitrogen content. The δ-$TiN_x$ exists between $x \approx 0.45$ and $x \approx 1.0$ ($x$ is the stoichiometric factor or the ratio of nitrogen to titanium). As can be seen, the nitrogen content increases as the implantation dose increases in the sub-stoichiometric range. At implantation doses above 2 to 4 $\times$ $10^{17}$ $N^+$-ions $cm^{-2}$ a saturation of the nitrogen content starts to appear. This is in accordance with what has been measured for other films prepared by reactive techniques [25] and bulk materials [26]. The nitrogen atoms occupy the interstitial octahedral sites in the α-Ti lattice and thus cause an expansion of this lattice. It is possible that up to the implanation of 5 $\times$ $10^{17}$ $N^+$-ions $cm^{-2}$ hyperstoichiometric compositions ($TiN_x$ with $x > 1$) are formed. Sometimes the high-flux implanted titanium layers have a dark colour due to a stoichiometric excess of nitrogen.

It should be noted that the δ-$TiN_x$ precipitates produced by high-flux nitrogen ion implantation ($\geqslant 5 \times 10^{17}$ $N^+$-ions $cm^{-2}$) have a preferential orientation. With the aid of special goniometer equipment in the HVEM, it was possible to determine microscopical inhomogeneities of texture. A fibrous arrangement of these nitrides was found. Exact calculations were prepared on the basis of incomplete pole figures [28].

In order to estimate the change of interplanar spacing of δ-$TiN_x$, it is necessary to determine the change of the lattice parameter of α-Ti. In Table III the measured interplanar spacings and relative intensities of the most intense electron diffraction reflections are compiled as a function of the implantation dose. From this table, it can be seen that the intensity and interplanar spacing increase with increasing implantation dose. In Fig. 4 the measured interplanar spacings of some reflections of α-Ti are plotted against the implantation dose of nitrogen. For implantation doses below 5 $\times$ $10^{16}$ to 1 $\times$ $10^{17}$ $N^+$-ions $cm^{-2}$ the lattice spacing increases as the implantation dose increases. Sundgren *et al.* [25] have also found that the interplanar spacing of titanium increases

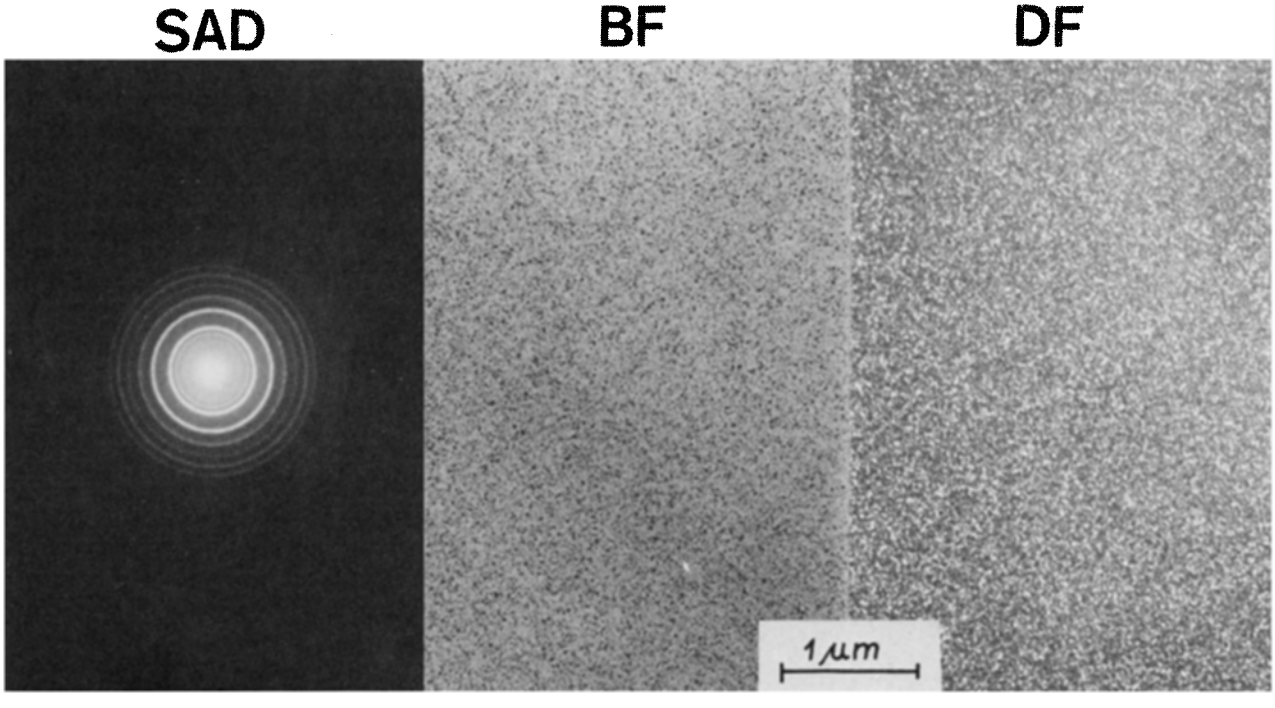


*Figure 2* Transmission electron diffraction pattern (SAD), bright field (BF) and dark field (DF) micrographs of titanium implanted with 50 keV nitrogen ions to a flux of 5 $\times$ $10^{16}$ $N^+$-ions $cm^{-2}$ at room temperature.

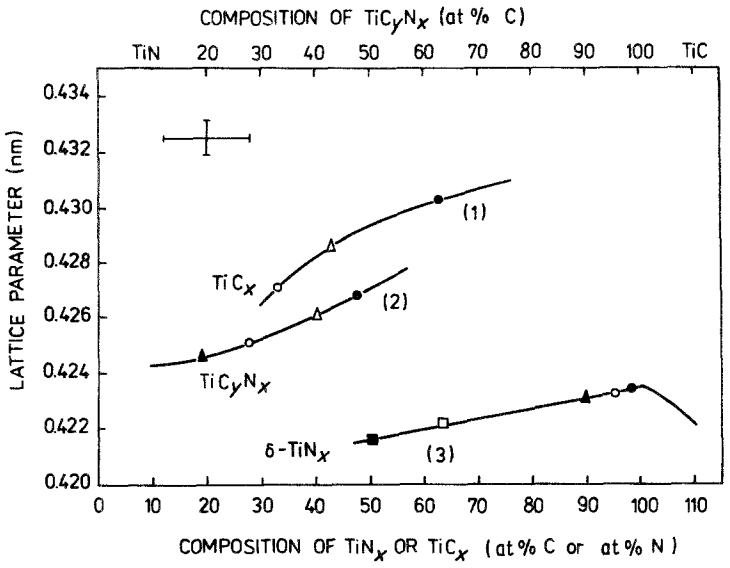


*Figure 3* Lattice parameters of $TiN_x$, $TiC_yN_x$ and $TiC_y$ layers as a function of composition. The solid lines (1) and (3) represent bulk results from Ehrlich [26] and the solid line (2) represents bulk results from Neshpor *et al.* [27]. Points demonstrate experimental lattice parameters of these titanium compounds formed by nitrogen ion implantation at 50 keV into titanium at different doses: (■) $5.0 \times 10^{16}$, (□) $1.0 \times 10^{17}$, (▲) $2.5 \times 10^{17}$, (○) $5.0 \times 10^{17}$, (●) $1.0 \times 10^{18}$ $N^+$-ions $cm^{-2}$.

with nitrogen content during reactive sputtering. The reason for this behaviour is not yet clear and further work is needed. It could possibly be due to (i) intrinsic stresses in the implanted films, and (ii) incorporation of oxygen during preparation of titanium films and/or carbon during implantation. However, no effect was noticed during AES measurements [9] in the dose range of 1 to $2.5 \times 10^{16}$ $N^+$-ions $cm^{-2}$.

At implantation doses above 1 to $2.5 \times 10^{17}$ $N^+$-ions $cm^{-2}$, reflections from the tetragonal ε-$Ti_2N$ phase start to appear beside the δ-$TiN_x$. Fig. 5 shows SAD with bright field (BF) and dark field (DF) micrographs of titanium implanted with $5 \times 10^{17}$ $N^+$-ions $cm^{-2}$. In Table I the values of the relevant parameters of the ε-$Ti_2N$ phase are listed. This phase is present only in a narrow composition range around 33 at %. The ε-$Ti_2N$ phase could be found after nitrogen ion implantation into α-Ti at

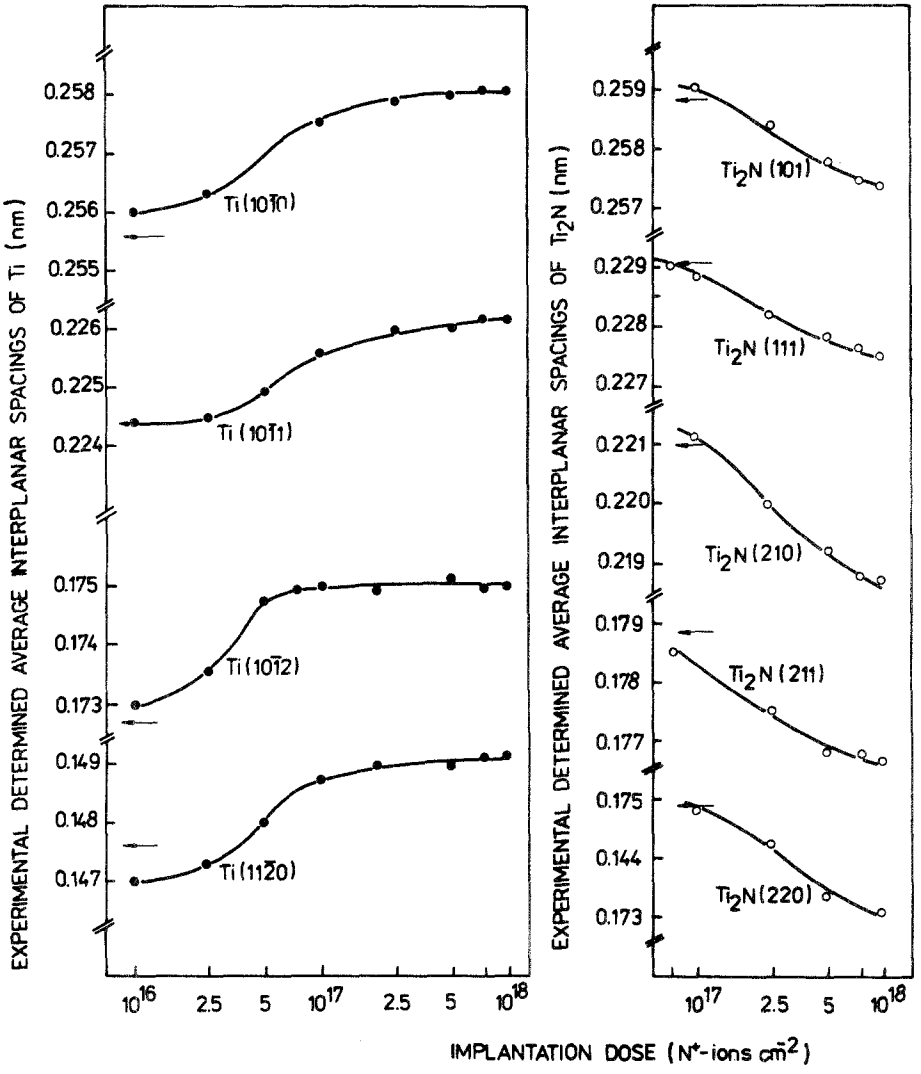


*Figure 4* Measured interplanar spacing as a function of the nitrogen ion implantation dose for α-Ti (left) and $Ti_2N$ (right) at room temperature and 50 keV implantation energy. Bulk values of the interplanar spacing for α-Ti and $Ti_2N$ are shown (arrows).

TABLE II Summary of most frequent lattice indices and intensities of $\delta$-$TiN_x$, with interplanar spacings used in calculation of $\varepsilon_d$

| Miller indices ($hkl$) | Theoretical interplanar spacing intensity | | | | Experimental interplanar spacing, intensity and deviation factor | | | | | |
|---|---|---|---|---|---|---|---|---|---|---|
| | $TiN_{0.6}$ | | $TiN_{1.0}$ | | $5 \times 10^{16}$ $N^+$-ions $cm^{-2}$ | | | $1 \times 10^{18}$ $N^+$-ions $cm^{-2}$ | | |
| | $d_{hkl}^{theo}$ (nm) | $I_{hkl}^{theo}$ | $d_{hkl}^{theo}$ (nm) | $I_{hkl}^{theo}$ | $d_{hkl}^{exp}$ (nm) | $I_{hkl}^{exp}$ | $\varepsilon_d$ (%) | $d_{hkl}^{exp}$ (nm) | $I_{hkl}^{exp}$ | $\varepsilon_d$ (%) |
| 111 | 0.2438 | 27.7 | 0.2449 | 29.9 | 0.243 | 24 | 0.11 | 0.245 | 32 | 0.05 |
| 200 | 0.2111 | 98 5 | 0.2121 | 100.0 | 0.211 | 85 | 0.05 | 0.212 | 100 | 0.05 |
| 220 | 0.1493 | 62.1 | 0.1500 | 65.4 | 0.148 | 58 | 0.87 | 0.150 | 65 | 0 |
| 311 | 0.1273 | 10.0 | 0.1279 | 11.1 | 0.127 | 5 | 0.24 | 0.129 | 9 | 0.86 |
| 222 | 0.1219 | 18.7 | 0.1225 | 20.9 | 0.122 | 18 | 0.08 | 0.122 | 23 | 0.41 |
| 400 | 0.1056 | 9.6 | 0.1060 | 9.6 | 0.105 | 8 | 0.57 | 0.106 | 12 | 0 |
| 331 | 0.0969 | 4.7 | 0.0974 | 4.6 | 0.097 | 5 | 0.10 | 0.098 | 5 | 0.62 |
| 420 | 0.0944 | 24.1 | 0.0948 | 23.4 | 0.094 | 20 | 0.42 | 0.094 | 21 | 0.84 |
| 422 | 0.0862 | 17.2 | 0.0866 | 16.2 | 0.085 | 13 | 1.39 | 0.086 | 17 | 0.69 |

room temperature in the dose range between $1 \times 10^{17}$ to $2.5 \times 10^{17}$ and $1.5 \times 10^{18}$ $N^+$-ions $cm^{-2}$. Table IV shows the interplanar spacings and intensities of the most frequent reflections of $\varepsilon$-$Ti_2N$ for two implantation doses. The experimental values are compared with theoretical data. From Table IV it can be seen that the measured intensities and interplanar spacings of the observed reflections decrease when the implantation dose increases. The dependence of the experimentally determined average interplanar spacings of the most intense electron diffraction reflections on implantation dose is shown in Fig. 4 (right). It confirms a tendency of the interplanar spacing to decrease with increasing implanted nitrogen dose. In the case of $\varepsilon$-$Ti_2N$ produced by reactive sputtering, Sundgren *et al.* [25] discussed whether high compressive stresses occur when nitrogen is incorporated. The tetragonal structure of $\varepsilon$-$Ti_2N$ has a low symmetry and it is therefore difficult to develop a non-stressed dense structure.

The average diameter of the implantation-induced titanium nitride grains depends on the implantation dose. A comparison of the dark fields of Figs. 2 and 5 demonstrates that the average diameter of precipitates after $5 \times 10^{16}$ $N^+$-ions $cm^{-2}$ implantation is increased to about 150 nm after implantation with $5 \times 10^{17}$ $N^+$-ions $cm^{-2}$. A further increase of diameter of precipitation with higher doses could not be found without thermal treatment [8].

At high implantation doses ($> 2.5$ to $5 \times 10^{17}$ $N^+$-ions $cm^{-2}$) analysis showed not only titanium nitrides but also titanium carbonitrides and titanium carbides. Also different THEED reflections (1 0 1), (2 0 0), (1 2 0) and (2 2 0), of rutile $TiO_2$ (tetrag.) could be detected in some cases. A dependence of the formation of rutile on implantation dose, temperature and vacuum conditions was not found. Because of carbon adsorption during the implantation process and recoil implantation by nitrogen ion bombardment the titanium layer is additionally doped with carbon. Measurements with the help of AES show that carbon is transported to a depth of 50 to 80 nm at doses $> 1 \times 10^{17}$ $N^+$-ions $cm^{-2}$ [8, 9]. It is known that carbon can occupy the lattice sites of nitrogen in metal carbonitride phases. For example, the implantation of nitrogen ions into iron leads to the formation of iron nitride phases [29, 30] and iron carbonitride phases [31].

Investigations of carbonitride phases are very difficult because the lattice parameters of these phases diverge only a little from the parameters of nitride phases and the electron diffraction intensities show only small differences; also the atomic scattering factors of nitrogen and carbon atoms are very similar. Fig. 6 shows SAD, bright field (BF) and dark field (DF) micrographs of titanium implanted with $1 \times 10^{18}$ $N^+$-ions $cm^{-2}$. According to Morrey [17] it is possible to identify and separate overlapped and densely packed peaks. Fig. 1 demonstrates this identification; some titanium carbonitride reflections could be found.

TABLE III Summary of most frequent lattice indices and intensities of $\alpha$-Ti after implantation at room temperature,

| Miller–Bravais indices ($hkil$) | Theoretical interplanar spacing and intensity | | Experimental interplanar spacing and intensity at different implantation doses ($N^+$-ions $cm^{-2}$) | | | | | | Deviation factor for $1 \times 10^{18}$ $N^+$-ions $cm^{-2}$, $\varepsilon_d$(%) |
|---|---|---|---|---|---|---|---|---|---|
| | | | $1 \times 16^{16}$ | | $1 \times 10^{17}$ | | $1 \times 10^{18}$ | | |
| | $d_{hkl}^{theo}$ (nm) | $I_{hkl}^{theo}$ | $d_{hkl}^{exp}$(nm) | $I_{hkl}^{exp}$ | $d_{hkl}^{exp}$(nm) | $I_{hkl}^{exp}$ | $d_{hkl}^{exp}$(nm) | $I_{hkl}^{exp}$ | |
| $10\bar{1}0$ | 0.2556 | 77.7 | 0.256 | 62 | 0.258 | 63 | 0.258 | 65 | 0.94 |
| $10\bar{1}1$ | 0.2244 | 100.0 | 0.224 | 95 | 0.226 | 96 | 0.226 | 100 | 0.71 |
| $10\bar{1}2$ | 0.1727 | 14.4 | 0.173 | 12 | 0.175 | 18 | 0.175 | 25 | 1.33 |
| $11\bar{2}0$ | 0.1476 | 17.1 | 0.147 | 15 | 0.149 | 23 | 0.150 | 32 | 1.63 |
| $10\bar{1}3$ | 0.1332 | 17.7 | 0.134 | 17 | 0.136 | 25 | 0.136 | 27 | 2.10 |
| $20\bar{2}1$ | 0.1233 | 13.6 | 0.122 | 14 | 0.124 | 13 | 0.123 | 15 | 0.24 |
| 0004 | 01171 | 8.0 | – | – | 0.120 | 6 | 0.120 | 8 | 2.48 |
| $20\bar{2}3$ | 0.0989 | 6.0 | – | – | 0.101 | 10 | 0.100 | 11 | 1.11 |
| $12\bar{3}1$ | 0.0946 | 4.9 | – | – | 0.095 | 6 | 0.097 | 7 | 2.54 |
| $30\bar{3}0$ | 0.0852 | 4.5 | – | – | 0.086 | 5 | 0.086 | 2 | 0.94 |

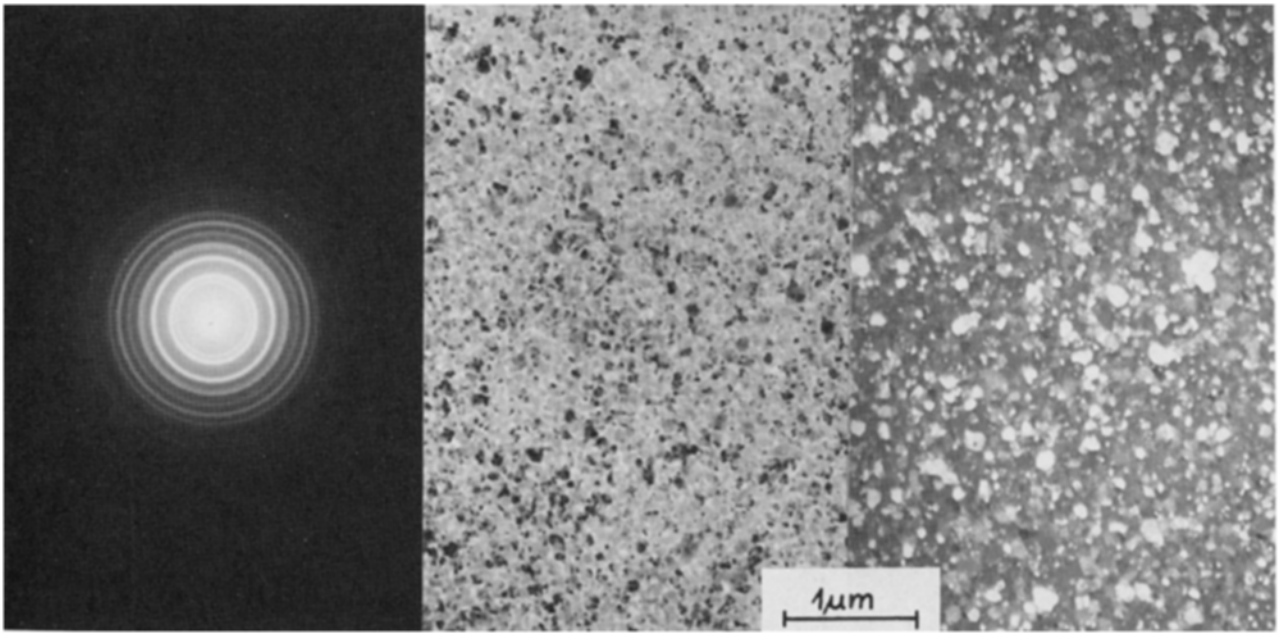


*Figure 5* Transmission electron diffraction pattern (SAD), bright field (BF) and dark field (DF) micrographs of titanium implanted with 50 keV nitrogen ions to a flux of $5 \times 10^{17}$ $N^+$-ions $cm^{-2}$ at room temperature.

Nitrogen ion implantation of titanium with high doses leads to the formation of cubic $TiC_yN_x$ and $TiC_x$. The structure of the titanium carbonitride phase is isomorphous with the $TiN_x$ phase. Nitrogen and carbon proportions in the octahedral (interstitial) positions of the face-centred cubic $TiC_yN_x$ phase are dependent on the implantation dose. It is not possible to distinguish the habit of $\delta$-$TiN_x$ and $TiC_yN_x$ precipitates in the bright or dark field of Fig. 6. Table V shows a comparison of the measured interplanar spacing of the most intense electron diffraction reflection of titanium implanted with different nitrogen ion doses with theoretical values of interplanar spacing for different compositions. The carbon content is found to increase with increasing implantation dose. On the basis of this comparison it is possible to estimate the concentration of carbon in the titanium carbonitride precipitates. For example, the carbon concentration is about 30 at % after the implantation of $1 \times 10^{18}$ $N^+$-ions $cm^{-2}$ into the carbonitride phases. AES analysis shows that the carbon concentration in the implanted layer is very much smaller than in the titanium carbonitride precipitates. Fig. 3 shows the variation of the lattice parameter of $TiC_yN_x$ with carbon and nitrogen concentration (points) together with data from Neshpor *et al.* [27] (solid line). The tendency described above is confirmed. It is probable that the high value of the lattice parameter is due to the incorporation of carbon into the lattice. The titanium carbonitride phase could be found after implantation of nitrogen ions with doses between 1 to $2.5 \times 10^{17}$ and $1.5 \times 10^{18}$ $N^+$-ions $cm^{-2}$.

A pure titanium carbide phase could be detected after implantation of nitrogen ions with a dose $> 5 \times$

TABLE IV Summary of most frequent lattice indices and intensities of $\varepsilon$-$Ti_2N$.

| Miller indices ($hkl$) | Theoretical interplanar spacing and intensity | | Experimental interplanar spacing, intensity and deviation factor | | | | | |
|---|---|---|---|---|---|---|---|---|
| | | | $2.5 \times 10^{17}$ $N^+$-ions $cm^{-2}$ | | | $1 \times 10^{18}$ $N^+$-ions $cm^{-2}$ | | |
| | $d^{theo}_{hkl}$ (nm) | $I^{theo}_{hkl}$ | $d^{exp}_{hkl}$ (nm) | $I^{exp}_{hkl}$ | $\varepsilon_d$ (%) | $d^{exp}_{hkl}$ (nm) | $I^{exp}_{hkl}$ | $\varepsilon_d$ (%) |
| 101 | 0.2587 | 100.0 | 0.259 | 100 | 0.12 | 0.257 | 95 | 0.66 |
| 200 | 0.2471 | 7.9 | 0.248 | 15 | 0.16 | 0.248 | 8 | 0.36 |
| 111 | 0.2292 | 74.0 | 0.229 | 86 | 0.09 | 0.228 | 78 | 0.52 |
| 210 | 0.2210 | 25.6 | 0.221 | 33 | 0 | 0.219 | 26 | 0.91 |
| 211 | 0.1787 | 87.6 | 0.179 | 72 | 0.17 | 0.177 | 68 | 0.95 |
| 220 | 0.1748 | 68.0 | 0.175 | 65 | 0.11 | 0.173 | 58 | 0.10 |
| 221 | 0.1515 | 2.7 | 0.150 | 1 | 0.99 | – | – | – |
| 301 | 0.1448 | 58.1 | 0.145 | 42 | 0.14 | 0.144 | 40 | 0.55 |
| 112 | 0.1392 | 30.2 | 0.139 | 36 | 0.14 | 0.138 | 37 | 0.86 |
| 311 | 0.1390 | 13.9 | | | 0 | | | 0.72 |
| 330 | 0.1165 | 34.9 | | | 2.18 | | | 2.15 |
| 222 | 0.1146 | 31.7 | 0.114 | 57 | 0.52 | 0.114 | 51 | 0.52 |
| 401 | 0.1145 | 19.4 | | | 0.44 | | | 0.52 |
| 312 | 0.1089 | 11.4 | 0.109 | 9 | 0.02 | 0.106 | 9 | 2.66 |
| 331 | 0.1088 | 0.9 | | | 0.18 | | | 2.57 |
| 412 | 0.0924 | 7.3 | 0.094 | 5 | 1.03 | – | – | – |

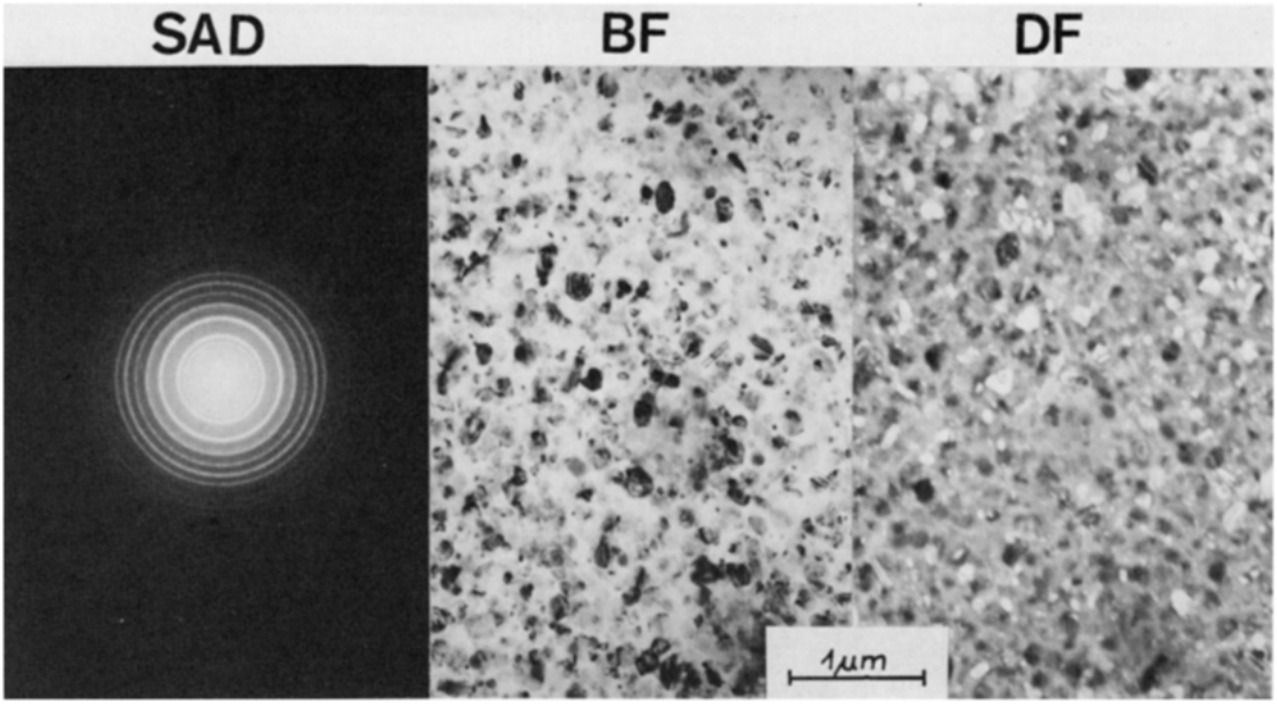


*Figure 6* Transmission electron diffraction pattern (SAD), bright field (BF) and dark field (DF) micrographs of titanium implanted with 50 keV nitrogen ions to a flux of $1 \times 10^{18}$ $N^+$-ions $cm^{-2}$ at room temperature.

$10^{17}$ $N^+$-ions $cm^{-2}$. Table VI shows the measured interplanar spacings and most intense electron diffraction reflections of titanium carbide formed by nitrogen ion implantation with doses of $5 \times 10^{17}$ and $1 \times 10^{18}$ $N^+$-ions $cm^{-2}$. These values are compared with theoretical data for $TiC_{0.35}$ and $TiC_{0.5}$. The phase $TiC_y$ is present for concentrations higher than 30 at % in the titanium carbide precipitates. If the concentration of carbon is lower then the carbon is dissolved into α-Ti and/or it occupies the interstitial octahedral nitrogen sites in the α-Ti. The lattice parameter for the $TiC_y$ phase, calculated from the measured interplanar spacings, is shown in Fig. 3. The lattice parameter varied between about 0.427 and 0.431 nm in the dose range between $5 \times 10^{17}$ and $1 \times 10^{18}$ $N^+$-ions $cm^{-2}$. The variation of the lattice parameter corresponds to a variation of composition from $TiC_{0.15}$ to $TiC_{0.3}$.

Titanium carbide and titanium carbonitride phases can be formed during nitrogen ion implantation if the concentration of carbon is sufficiently high. A high carbon concentration can be caused by high-flux implantation and high times of implantation respectively. This fact is demonstrated in Fig. 7. This figure shows small portions of electron scattering curves of titanium implanted with different nitrogen doses. From Fig. 7 it can be seen that δ-$TiN_x$ is formed only after implantation of $5 \times 10^{16}$ $N^+$-ions $cm^{-2}$. A second phase (ε-$Ti_2N$) appears after implantation of $2.5 \times 10^{17}$ $N^+$-ions $cm^{-2}$. A comparison of these two electron scattering curves shows the shift of reflection peaks (2 0 0)-$TiN_x$, (1 1 1)-$Ti_2N$ and (2 1 0)-$Ti_2N$ as a function of the implantation dose. At higher nitrogen ion implantation doses the reflection peaks (2 0 0)-$TiC_yN_x$ (after implanatation of $5 \times 10^{17}$ $N^+$-ions $cm^{-2}$) and (2 0 0)-$TiC_y$ (after implantation of $1 \times 10^{18}$ $N^+$-ions $cm^{-2}$) can be found. In this figure it is also shown that the observed electron reflection peaks of the titanium carbonitride phase and titanium carbide phase are shifted in their dependence on implantation dose.

On the basis of these invesitgations a "state diagram" or a diagram of existence range can be drawn. In Fig. 8 this diagram is represented. As opposed to the equilibrium phase diagram at room temperature it includes metastable phases and partially violates the Gibbs phase rule. Such state diagrams are known from the systems boron/iron [16] and nitrogen/iron [16, 30]. The cause of this behaviour must be sought in

TABLE V Comparison of calculated interplanar spacings for four different $TiC_yN_x$ compounds with experimentally measured values

| Miller indices ($h\,k\,l$) | Theoretical interplanar spacing $d_{hkl}^{theo}$ (nm) for different $TiC_yN_x$ | | | | Experimental interplanar spacing $d_{hkl}^{exp}$ (nm) at different implantation doses ($N^+$-ions $cm^{-2}$) | | |
|---|---|---|---|---|---|---|---|
| | $TiC_{0.04}N_{0.87}$ | $TiC_{0.14}N_{0.77}$ | $TiC_{0.41}N_{0.5}$ | $TiC_{0.61}N_{0.31}$ | $2.5 \times 10^{17}$ | $5 \times 10^{17}$ | $1 \times 10^{18}$ |
| 1 1 1 | 0.2447 | 0.2454 | 0.2469 | 0.2481 | 0.245 | 0.245 | 0.247 |
| 2 0 0 | 0.2119 | 0.2125 | 0.2138 | 0.2148 | 0.212 | 0.212 | 0.214 |
| 2 2 0 | 0.1498 | 0.1503 | 0.1512 | 0.1519 | 0.150 | 0.151 | 0.151 |
| 3 1 1 | 0.1278 | 0.1283 | 0.1289 | 0.1296 | – | 0.128 | 0.129 |
| 2 2 2 | 0.1223 | 0.1227 | 0.1235 | 0.1240 | 0.122 | 0.123 | 0.123 |
| 4 0 0 | 0.1059 | 0.1063 | 0.1069 | 0.1074 | – | 0.106 | 0.107 |

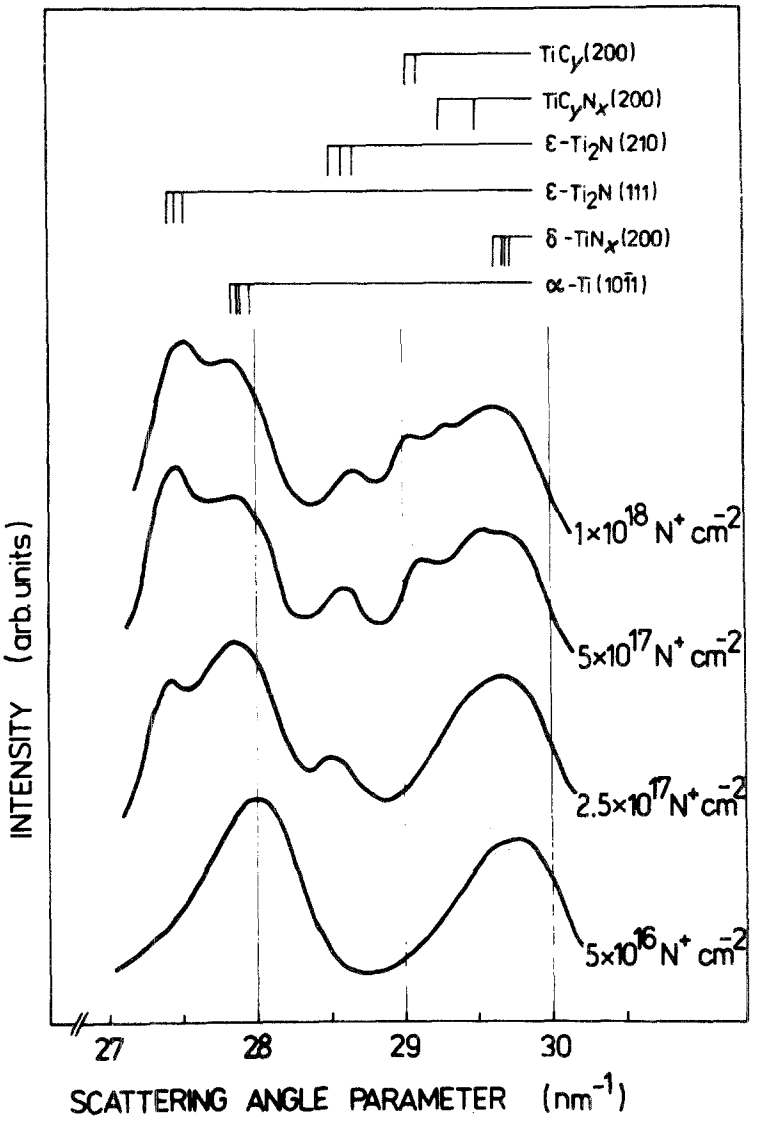


*Figure 7* Electron scattering intensity against scattering angle parameter between 27 and 30 nm$^{-1}$ for titanium after implantation with different nitrogen ion doses at 50 keV implantation energy and room temperature.

the themodynamical non-equilibrium process of ion implantation (for discussion see [29–33]. The results of nitrogen ion implantation-induced titanium nitride formation agree well with the few published results [4–7].

At present the process of implantation-induced phase formation is not clear. In this work, it was demonstrated that nitrogen ion implantation into titanium at room temperature leads to the formation of different titanium nitride and titanium carbide phases. Under conventional conditions very high temperatures are necessary for the formation of these phases; for example, the melting point of δ-TiN is about 3000° C. The explanations that have been proposed for formation of compounds by ion implantation include cascade effects [29, 30, 34, 35], radiation damage [36], and themodynamical and chemical forces [37, 28].

## 4. Conclusions

It was shown in this work that high-flux nitrogen ion implantation into titanium at room temperature leads to the formation of different titanium nitride, titanium carbonitride, titanium carbide and titanium oxide

TABLE VI Summary of most frequent lattice indices and intensities of TiC$_y$, with interplanar spacings used in calculation of $\varepsilon_d$

| Miller indices ($hkl$) | Theoretical interplanar spacing and intensity | | | | Experimental interplanar spacing, intensity and deviation factor | | | | | |
|---|---|---|---|---|---|---|---|---|---|---|
| | TiC$_{0.35}$ | | TiC$_{0.5}$ | | 5 × 10$^{17}$ N$^+$-ions cm$^{-2}$ | | | 1 × 10$^{18}$ N$^+$-ions cm$^{-2}$ | | |
| | $d_{hkl}^{theo}$ (nm) | $I_{hkl}^{theo}$ | $d_{hkl}^{theo}$ (nm) | $I_{hkl}^{theo}$ | $d_{hkl}^{exp}$(nm) | $I_{hkl}^{exp}$ | $\varepsilon_d$(%) | $d_{hkl}^{exp}$(nm) | $I_{hkl}^{exp}$ | $\varepsilon_d$(%) |
| 111 | 0.2486 | 31.6 | 0.2498 | 33.6 | 0.246 | 29 | 1.05 | 0.249 | 35 | 0.30 |
| 200 | 0.2152 | 98.0 | 0.2163 | 100.0 | 0.213 | 94 | 1.02 | 0.216 | 100 | 0.14 |
| 220 | 0.1522 | 77.3 | 0.1530 | 78.9 | 0.151 | 73 | 0.79 | 0.153 | 76 | 0 |
| 311 | 0.1298 | 12.7 | 0.1305 | 14.0 | 0.129 | 10 | 0.62 | 0.132 | 12 | 1.15 |
| 222 | 0.1243 | 16.1 | 0.1249 | 17.9 | 0.123 | 21 | 1.04 | 0.124 | 19 | 0.72 |
| 400 | 0.1076 | 6.6 | 0.1082 | 7.4 | 0.107 | 8 | 0.56 | 0.109 | 7 | 0.74 |
| 331 | 0.0988 | 4.2 | 0.0993 | 4.5 | 0.098 | 5 | 0.81 | 0.101 | 5 | 1.71 |
| 420 | 0.0963 | 19.1 | 0.0967 | 20.9 | 0.095 | 18 | 1.34 | 0.096 | 22 | 0.72 |
| 422 | 0.0879 | 13.6 | 0.0883 | 15.5 | 0.087 | 11 | 1.02 | 0.088 | 19 | 0.33 |

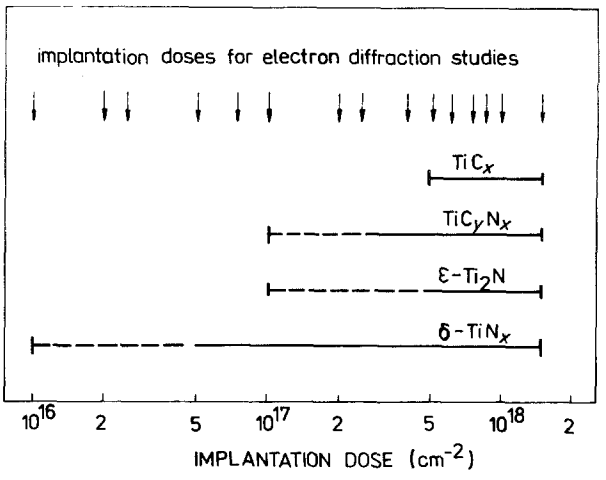


*Figure 8* Titanium nitride, titanium carbide and titanium carbonitride phases as a function of implantation doses (state diagram) for 30 to 60 keV $N^+$ ions. Arrows indicate the implanation dose at which electron diffraction measurements were made.

phases. The formation of these phases is a function of implantation dose. $\delta$-$TiN_x$ is found in the dose range from $1 \times 10^{16}$ up to $1.5 \times 10^{18}$ $N^+$-ions cm$^{-2}$. The stoichiometrical factor $x$ varies between about 0.45 and 1.0, depending on implantation dose. A hyperstoichiometrical composition ($x > 1$) is also possible. $\varepsilon$-$Ti_2N$ is observed in the dose range between 1 to $2.5 \times 10^{17}$ and $1.5 \times 10^{18}$ $N^+$-ions cm$^{-2}$ in addition to $\delta$-$TiN_x$. The measured interplanar spacings of this phase decrease when the implantation dose increases. The titanium target is additinally doped with carbon, because carbon adsorption and recoil implantation during the implantation process occurs by nitrogen ion bombardment. Therefore at high implantation doses ($> 2.5$ to $5 \times 10^{17}$ $N^+$-ions cm$^{-2}$) there was evidence for titanium carbonitride $TiC_yN_x$ and titanium carbide $TiC_y$. The structure of these carbonitride and carbide phases are dependent on implantation dose, i.e. on the ratio of nitrogen to carbon.The existence ranges of the titanium phases can be expressed in a state diagram.

## Acknowledgements

The author would like to thank Dr J. Schöneich and Mr J. Altmann for performing the implantations, Professor H. Bethge and Dr G. Kästner (Institute for Solid State Physics and Electron Microscopy, Halle/Saale for help with the HVEM investigations, Mrs G. Otto for help in programming the computer and Professor K. Hohmuth for stimulating discussions concerning the problems of phase formation by ion implanation.

## References

1. G. DEARNALEY, *Thin Solid Films* **107** (1983) 315.
2. C. F. POWELL, J. H. OXLEY and J. M. BLOCHER, "Vapour Deposition" (Wiley, New York, 1966).
3. A. K. SURI, R. NIMMAGADDA and R. F. BUNSHAH, *Thin Solid Films* **72** (1980) 529.
4. V. N. BYKOV, V. A. TROYAN, G. G. ZDOROVTSEVA and V. S. KHAIMOVICH, *Phys. Status Solidi (a)* **32** (1975) 53.
5. M. BELII, F. F. KOMAROV, V. S. TISHKOV and V. M. YANKOVSKII, *ibid.* **45** (1978) 343.
6. P. A. CHEN and T. T. YANG, *Thin Solid Films* **81** (1981) L91.
7. R. G. DUCKWORTH and I. H. WILSON, *ibid.* **63** (1979) 289.
8. K. HOHMUTH and B. RAUSCHENBACH, *Mater. Sci. Eng.* **69** (1985) 489.
9. B. RAUSCHENBACH, G. BLASEK and R. DIETSCH, *Phys. Status Solidi (a)* **85** (1984) 473.
10. K. W. ANDREWS, D. J. DYSON and S. K. KEOWN "Interpretation of Electron Diffraction Patterns" (Hilger and Watts, London, 1971) p. 21.
11. Z. G. PINSKER, "Electron Diffraction" (Butterworth, London, 1953) p. 214.
12. "International Tables for X-ray Crystallography", Vol. I (The Kynoch Press, Birmingham, 1962).
13. J. W. EDINGTON, "Practical Electron Microscopy in Materials Science" (Macmillan, London, 1976) p. 113.
14. J. A. IBERS, *Acta Crystallogr.* **11** (1957) 86.
15. K. HERRMANN, *Krystallogr.* **68** (1928) 288.
16. K. HOHMUTH, B. RAUSCHENBACH and E. RICHTER, *Nucl. Inst. Meth.* **209/210** (1983) 249.
17. J. R. MORREY, *Anal. Chem.* **40** (1968) 905.
18. P. QUITTNER, "Gamma-Ray Specroscopy with Particular Reference to Detector and Computer Evaluation Techniques" (Akademini Kiado, Budapest, 1972) p. 30.
19. G. WILL, W. PARRISH and T. C. HUANG, *J. Appl. Crystallogr.* **16** (1983) 611.
20. M. HANSEN, "Constitution of Binary Alloys" (McGraw-Hill, New York, 1958) p. 989.
21. P. ROGL, "Atomic Energy Reveiw, Special Issue No. 9" (IAEA, Wien, 1983) p. 201.
22. H. F. FRAZEN, *ibid.*, p. 371.
23. H. HOLLECK, Binäre und ternäre Carbide und Nitride der Übergangsmetalle und ihre Phaserbeziehungen Kernforschungszentrum Karlsruhe, "KfK-Report 3087 B" (1981).
24. A. ARMIGLIATO, G. CELOTTI, A. GARULLI, S. GUERRI, P. OSTOJA, R. ROSA and G. MARTINELLI, *Thin Solid Films* **92** (1982) 341.
25. J.-E. SUNDGREN, B.-O. JOHANSSON, S.-E. KARLSSON and H. T. G. HENTZEL, *ibid.* **105** (1983) 367.
26. P. EHRLICH, *Z. Anorg. Chem.* **259** (1949) 1.
27. V. S. NESHPOR, G. M. KLIMASHIN and V. P. NIHITIN, "Refractory Carbides", edited by G. V. Samsonov (Plenum Press, New York, 1974) p. 341.
28. B. RAUSCHENBACH and K. HELMING, in preparation.
29. B. RAUSCHENBACH and A. KOLITSCH, *Phys. Status Solidi (a)* **80** (1983) 211.
30. B. RAUSCHENBACH, A. KOLITSCH and K. HOHMUTH, *ibid.* **80** (1983) 471.
31. B. RAUSCHENBACH and K. HOHMUTH, *Cryst. Res. Technol.* **19** (1984) 1425.
32. S. T. PICRAUX and W. J. CHOYKE, "Metastable Materials Formation by Ion Implantation" (North-Holland, New York, 1982).
33. J. W. POATE and A. G. CULLIS, "Treatise on Materials Science and Technology", Vol. 18, edited by J. K. Hirvonen (Academic Press, New York, 1980) p. 85.
34. B. RAUSCHENBACH and K. HOHMUTH, *Phys. Status Solidi* (a) **75** (1983) 159.
35. P. ZIEMAN, *Mater. Sci. Eng.* **69** (1985) 95.
36. E. N. KAUFMANN and L. BUENE, *Nucl. Instr. Meth.* **182/183** (1981) 327.
37. J. A. BORDERS, *Ann. Rev. Mater. Sci.* **9** (1979) 313.
38. A. D. MARWICK, *Nucl. Instr. Meth.* **182/183** (1981) 827.

*Received 7 January*
*and accepted 21 February 1985*